Energy & Environmental Science

Cite this: *Energy Environ. Sci.*, 2012, **5**, 8359

www.rsc.org/ees

PAPER

Zeolitic imidazolate framework (ZIF-8) based polymer nanocomposite membranes for gas separation†

Qilei Song,[a] S. K. Nataraj,[a] Mina V. Roussenova,[b] Jin Chong Tan,[c] David J. Hughes,[b] Wei Li,[c] Pierre Bourgoin,[a] M. Ashraf Alam,[b] Anthony K. Cheetham,[c] Shaheen A. Al-Muhtaseb[d] and Easan Sivaniah*[a]

Received 19th April 2012, Accepted 12th June 2012
DOI: 10.1039/c2ee21996d

As synthesised ZIF-8 nanoparticles (size ~ 60 nm and specific surface area ~ 1300–1600 $m^2 g^{-1}$) were directly incorporated into a model polymer matrix (Matrimid® 5218) by solution mixing. This produces flexible transparent membranes with excellent dispersion of nanoparticles (up to loadings of 30 wt%) with good adhesion within the polymer matrix, as confirmed by scanning electron microscopy, dynamic mechanical thermal analysis and gas sorption studies. Pure gas (H_2, CO_2, O_2, N_2 and CH_4) permeation tests showed enhanced permeability of the mixed matrix membrane with negligible losses in selectivity. Positron annihilation lifetime spectroscopy (PALS) indicated that an increase in the free volume of the polymer with ZIF-8 loading together with the free diffusion of gas through the cages of ZIF-8 contributed to an increase in gas permeability of the composite membrane. The gas transport properties of the composite membranes were well predicted by a Maxwell model whilst the processing strategy reported can be extended to fabricate other polymer nanocomposite membranes intended for a wide range of emerging energy applications.

1. Introduction

Developing energy-efficient and environmentally friendly separation processes has become an important research topic in dealing with global issues such as CO_2 capture, natural gas purification and water purification. Membrane separation technology has great potential as an alternative to conventional industrial processes, with lower energy costs and fewer environmental impacts.[1] Conventional polymer membranes suffer from a trade-off between permeability and selectivity, *i.e.* polymers with high selectivity present low permeability and *vice versa*.[2] Such a trade-off behaviour can be captured *via* an empirical upper bound relationship as summarised by Robeson in 1991[3] and subsequently updated in 2008.[4] There have been extensive efforts during the last three decades to enhance the permeability and selectivity of polymeric membranes,[5] by (i)

[a]*Biological and Soft Systems Sector, Cavendish Laboratory, University of Cambridge, Cambridge CB3 0HE, UK. E-mail: es10009@cam.ac.uk; Fax: +44 (0)1223 337000; Tel: +44 (0)1223 337267*
[b]*H. H. Wills Physics Laboratory, University of Bristol, Tyndall Avenue, Bristol BS8 1TL, UK*
[c]*Department of Material Science and Metallurgy, University of Cambridge, Cambridge CB2 3QZ, UK*
[d]*Department of Chemical Engineering, Qatar University, P.O. Box 2713, Doha, Qatar*

† Electronic supplementary information (ESI) available: Summary of gas permeation data of pure ZIF membranes in the literature, gas permeation apparatus, characterisation of ZIF-8, including SEM, XRD, STEM, N_2 adsorption and desorption, characterisation of composite membranes including photos, SEM, XRD, FTIR and DMA data, detailed gas permeation data of the pure Matrimid® membrane and composite membranes, solubility and diffusion coefficient data. See DOI: 10.1039/c2ee21996d

Broader context

Membrane gas separation has attracted significant interest in recent years to match an urgent need for an energy-efficient technology for industrial applications such as natural gas purification and CO_2 capture. In this study, we report a method of dispersing nanoporous zeolitic imidazolate framework (ZIF-8) nanoparticles in a polymer matrix using colloidal solution mixing yielding excellently dispersed nanocomposites even at high loadings of nanoparticles. The method of dispersion is attractive in its simplicity and applicability to a wide combination of similar materials. The mixed matrix membranes showed significantly enhanced gas permeability whilst the membrane selectivity to important gases remained high and constant. This is of particular advantage in reducing the energy requirements for these key membrane separation processes and highlights the potential of metal–organic framework (MOF)-based nanocomposite membranes for gas separation.

design of new membrane materials using polymer chemistry,[6–13] (ii) post treatment of membranes by thermal rearrangement,[14] crosslinking by chemical or photochemical routes,[15] and (iii) mixed matrix membranes with porous or non-porous fillers.[16–18] With the development of nanotechnology and advanced materials over the past decade, there is a significant research interest in developing the next-generation nanoporous membranes for gas and liquid separation processes.[19,20] By tuning the pore size to match the kinetic diameter of chemical molecules and by tailoring chemical affinity towards specific molecules, both the permeability and selectivity properties are expected to be enhanced.[9,14,19–21]

Metal–organic frameworks (MOFs) are a relatively new family of nanoporous materials which are produced from metal ions or clusters linked by organic molecules.[22–24] Many MOF-type materials with diverse framework architectures and functional properties have been synthesised to date.[25–29] Zeolitic imidazolate frameworks (ZIFs) are a sub-family of MOFs that have tuneable pore sizes and chemical functionality, coupled with exceptional chemical stability, and exhibit versatile structures analogous to that of inorganic zeolites.[30] Particularly, several ZIFs have been successfully prepared as membranes and have demonstrated the molecular sieving effect needed for gas separation.[31–40] For example, ZIF-8 is made from linking of zinc(II) cations and 2-methylimidazole anions, giving a sodalite topology with a pore cavity of 11.6 Å and a theoretical pore aperture of 3.4 Å.[41] ZIF-8 has been demonstrated as capable of separating smaller gas molecules from larger ones, such as separation of H_2 from CH_4 (selectivity of 11–14),[33,42] separation of H_2 from hydrocarbons,[35] separation of CO_2 from CH_4 (relatively lower selectivity of 4–7).[31] By similar preparation techniques, some other ZIFs, including ZIF-7 (pore aperture ~ 3.0 Å), ZIF-22 (~3.0 Å), and ZIF-90 (~3.5 Å), have also been demonstrated as molecular sieving membranes.[32,34,36–38] Representative data are summarised in the ESI(Table S1†). However, the selectivities of these membranes are not yet satisfactory for industrial-scale applications. Another issue for these pure MOF-based membranes is the challenge of scaling up, which has been encountered by zeolite membranes. Although much progress has been made on zeolite membranes on the laboratory scale,[43] they have not yet found industrial applications in the field of gas separation, mainly because of the challenges of fabrication on large scale without pinholes or cracks.[44,45] Similarly, these challenges need to be resolved in the case of scale up of MOF-based membranes for gas separation processes.[44,45]

A promising application of MOFs is in the fabrication of mixed matrix membranes, or nanocomposite membranes, by incorporating nanoporous MOFs into a polymer matrix.[46–53] Mixed matrix membranes could combine the molecular sieving effect of MOFs and processability of the base polymers. Therefore, they could be readily scaled up for industrial applications using the established fabrication techniques for polymer membranes. Recently, several MOF-based mixed matrix membranes have been reported, such as MOF-5 in Matrimid®,[47] Cu–4,4′-bipyridine–hexafluorosilicate (Cu–BPY–HFS) in Matrimid®,[48] $Cu_3(BTC)_2$, BTC = 1,3,5-benzenetricarboxylate (also known as HKUST-1) in Matrimid®.[49] Generally, these studies showed that the gas permeability was enhanced whilst the selectivity was maintained approximately to that of the pure polymer in most cases. However, the aggregation and poor interfaces between MOFs and polymer matrix, as observed by scanning electron microscopy (SEM), suggested that defects could give an illusory enhancement of permeability whilst the inherent gas permeation properties of the composite membranes were not clear.

Recently, ZIFs gained attention as fillers for mixed matrix membranes because of their molecular sieving effect, facile synthesis and good compatibility with polymers. Bae *et al.*[51] synthesised ZIF-90 particles with sub-micrometer size and incorporated them into several polyimide polymers (Ultem® polyetherimide, Matrimid®, and 6FDA-DAM). The ZIF-90/6FDA-DAM membrane exhibited higher CO_2 permeability of 720 Barrer with a CO_2/CH_4 selectivity of 37 reaching the Robeson's upper bound. Using similar techniques, Zhang *et al.*[52] reported high C_3H_6/C_3H_8 separation performance of a ZIF-8/6FDA-DAM mixed matrix membrane. Ordoñez *et al.*[53] studied the Matrimid®–ZIF-8 mixed matrix membrane by incorporating ZIF-8 nanoparticles into the Matrimid® polymer. The permeability of these membranes was enhanced with increasing loading of ZIF-8 up to 40 wt% (loading with respect to polymer instead of membrane). The ZIF-8 nanocrystals were relatively large (>100 nm) and aggregated in the polymer with evident interfacial voids observed from the published SEM images. In a recent work, a ZIF-8/PMPS (polymethylphenylsiloxane) composite membrane shows promising separation of alcohols.[54] In summary, these studies have shown that there are several outstanding issues pertaining to polymer–MOFs nanocomposite membranes: (i) controlled synthesis of the sub-micrometer MOF nanoparticles, (ii) defect-free interface between polymers and MOFs, and (iii) controlled dispersion of MOFs within the polymer.

As introduced above, ZIF-based membranes have shown molecular sieving effect with high permeability. However, both the size and uniformity of the ZIFs nanoparticles as well as their effective dispersion in a polymer matrix remain to be improved. Furthermore, the effect of incorporation of ZIFs into the composite membrane on the mechanism of gas transport has yet to be elucidated. These fundamental issues will be addressed in the present work using ZIF-8 as a model of ZIFs, a well-studied polyimide, Matrimid®, as the model polymer matrix and a novel direct solution mixing of components to ensure a well-dispersed, highly loaded mixed matrix membrane.

2. Experimental

2.1. Materials

Commercially available glassy polyimide Matrimid® 5218 (see Fig. 1) was kindly provided by Huntsman Advanced Materials. The molecular weight of the as received polymer was M_n = 44 000 g mol^{-1} with a polydispersity index of 1.84, as analysed by gel permeation chromatography (GPC) calibrated by polystyrene standards. Zinc nitrate hexahydrate [$Zn(NO_3)_2 \cdot 6H_2O$] was obtained from Alfa Aesar and 2-methylimidazole [$C_4H_6N_2$] was obtained from Sigma-Aldrich. Methanol (Fisher Scientific) was used as solvent for the synthesis of ZIF-8 (see Fig. 1). Chloroform (Fisher Scientific) was used as solvent for the polymer. All chemicals were used as received without further

purification. Pure gases of H_2 (99.9995 vol%), CO_2 (99.995 vol%), O_2 (99.6 vol%), N_2 (99.9995 vol%) and CH_4 (99.5 vol%) (BOC, UK) were used for the gas permeation experiments.

2.2. Synthesis of ZIF-8 nanocrystals

The ZIF-8 nanocrystals were synthesised following the rapid room temperature synthesis method reported by Cravillon *et al.*[55] In a typical synthesis, a solution of 3 g (10 mmol) of $Zn(NO_3)_2 \cdot 6H_2O$ in 100 mL of methanol and another solution of 6.6 g (80 mmol) of 2-methylimidazole in 100 mL of methanol were prepared and then mixed by vigorously stirring for 1 h at room temperature. After 1 h stirring, the resulting ZIF-8 nanocrystals were separated by centrifugation, followed by washing with methanol twice and with chloroform once and finally re-dispersing as colloids in fresh chloroform for use in membrane preparation. As control samples, two batches of ZIF-8 nanocrystals were dried under vacuum at 60 °C and 230 °C for 18 h and stored dry for further analysis. The yield of ZIF-8 was about 40 mol% based on the ideal molar conversion of zinc.

2.3. Preparation of ZIF–polymer nanocomposite membrane

The Matrimid® 5218 polymer was dried in a vacuum oven at 110 °C overnight, dissolved in chloroform (20 wt%) at room temperature and stirred for 1–2 days until a clear solution was obtained. The as-synthesised ZIF-8 colloidal solution in chloroform with known concentration of ZIF-8 was further sonicated to prevent particulate aggregation. The Matrimid® and ZIF-8 solutions were mixed in ratios to control the MOF–polymer weight loading and stirred overnight. The concentration of the polymer in the final solution was adjusted to around 10 wt % by evaporation of excess solvent giving enough viscosity so that aggregation and sedimentation of ZIF-8 particles were minimised during membrane casting. After sonication to remove the air bubbles, the resulting polymer–ZIF-8 solution was cast onto a clean glass substrate and placed in a glove bag with saturated chloroform vapour to control the overnight drying of the polymer film. The membranes were removed from the glass substrate and annealed over the temperature range of 60–300 °C for 18 h under vacuum before slow cooling to room temperature; these membranes were stored dry prior to gas permeation and structure characterisation. The weight loading of ZIF-8 nanocrystals in the nanocomposite membrane was defined as $R_{ZIF\text{-}8} = m_{ZIF\text{-}8}/(m_{ZIF\text{-}8} + m_{polymer}) \times 100\%$. Nanocomposite membranes were prepared with loadings of ZIF-8 nanoparticles at 5, 10, 20, 30, and 40 wt%. Flat sheet dense membranes were prepared in A4-paper size. For the highest loading of 40 wt%, the membrane was very brittle and cracked into small pieces, which were not big enough for the gas permeation test. The thickness of the final pure and composite membranes varied within the range of 40–70 μm, depending on the loading of ZIF-8 and annealing conditions as measured by a micrometer (HITEC, Model 190-00, 0–25 mm, resolution 1 μm).

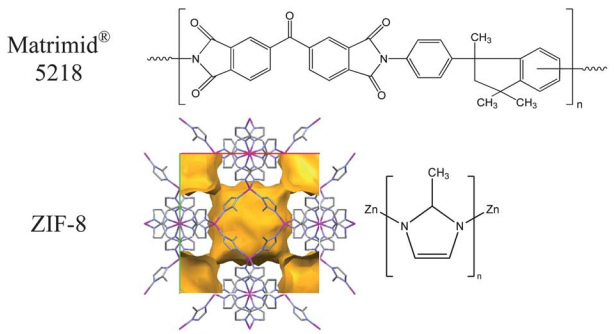

Fig. 1 Chemical structure of the polyimide Matrimid® 5218 and the ZIF-8 nanocrystals.

2.4. Characterisation of the materials

The volume fraction ϕ_D of ZIF-8 in the nanocomposite membrane is defined as:

$$\phi_D = \frac{m_D/\rho_D}{m_D/\rho_D + m_C/\rho_C} \quad (1)$$

where m and ρ refer to the mass and density of the continuous phase (polymer) and dispersed phase (ZIF-8), respectively, denoted by subscripts "C" and "D". As verified by SEM and gas sorption, the void volume could be neglected in most cases. Therefore, this apparent volume fraction is approximate to the true volume fraction of the ZIF-8 in the nanocomposite membrane.

Scanning electron microscopy (SEM) and scanning transmission electron microscopy (STEM) were performed using a Hitachi S5500 microscope. Samples were prepared by freeze-fracture of the membrane and subsequent sputter-coating with a thin layer of gold.

Wide angle X-ray diffraction (XRD) was performed with a Bruker D8 X-ray diffractometer operated at 40 mA and 40 kV using Cu Kα radiation with a step of 0.02° s^{-1}. The membrane sample was attached onto a sample holder with a single crystal silicon substrate. For the nanocomposite membrane containing ZIF-8, the average crystallite size of ZIF-8 is calculated from the Scherrer equation.[56]

Fourier transform infrared spectroscopy (FTIR) was performed on a NICOLET FTIR (iS10, Thermo Scientific) over the wavelength range of 400–4000 cm^{-1}, with a spectral resolution of 0.24 cm^{-1} and 64 scans. The thin nanocomposite membrane films (annealed at 230 °C for 18 h under vacuum) were measured directly whereas the ZIF-8 nanoparticles were prepared in KBr pellets, both under the transmission mode.

The glass transition temperatures (T_g) of the membranes were measured by a dynamic mechanical thermal analyser (DMA, Gearing Scientific Ltd.). A piece of ~3 × 5 mm^2 membrane was sandwiched in a stainless steel envelope (Triton Technology Material Pocket) which was then mounted in the analyser. Then the sample was heated from room temperature to 400 °C at a heating rate of 10 °C min^{-1} under a dynamic force with a single frequency oscillation of 1 Hz and at an amplitude of 50 μm. The storage modulus, phase angle and tan delta (ratio of storage modulus to loss modulus) were measured as functions of temperature and T_g was calculated from the peak of tan delta. For each sample, two or three pieces of the film were tested which gave good reproducibility of T_g (±2 °C).

The specific surface area and pore size distribution of the ZIF-8 nanoparticles were determined from the nitrogen adsorption

Table 1 Physical and chemical characteristics of Matrimid®–ZIF-8 nanocomposite membranes and pure ZIF-8 nanocrystals. All samples were annealed at 230 °C for 18 h under vacuum

$R_{ZIF\text{-}8}$ (wt%)	$\phi_{ZIF\text{-}8}$ (vol%)[a]	ρ_t (g cm^{-3})[b]	ρ_b (g cm^{-3})[c]	T_g (°C)	$L_{(ZIF\text{-}8)}$ (nm)[d]	S_{BET} (m^2 g^{-1})[e]
0	0	1.20	1.23 ± 0.03	330	—	—
5	6.2	1.19	1.15 ± 0.04	336	57 ± 2	—
10	12.3	1.18	1.13 ± 0.04	346	45 ± 1	—
20	24.0	1.15	1.10 ± 0.03	343	59 ± 1	~0.9
30	35.1	1.13	1.12 ± 0.04	349	46 ± 1	—
40	45.7	1.10	—	—	60 ± 2	—
100	100	0.95	—	—	69 ± 2	1358

[a] Volume fraction of ZIF-8. [b] Theoretical density of the composite membrane calculated by the mass ratio of ZIF-8 and polymer. The density of the Matrimid® 5218 polymer is 1.2 g cm^{-3} and the theoretical density of ZIF-8 is about 0.95 g cm^{-3}.[41] [c] Bulk density as quantified by measurement of weight and volume of the membranes, error was mainly subject to the uncertainty of thickness. [d] Crystallite size calculated from XRD data by the Scherrer equation. [e] BET surface area measured by N_2 adsorption.

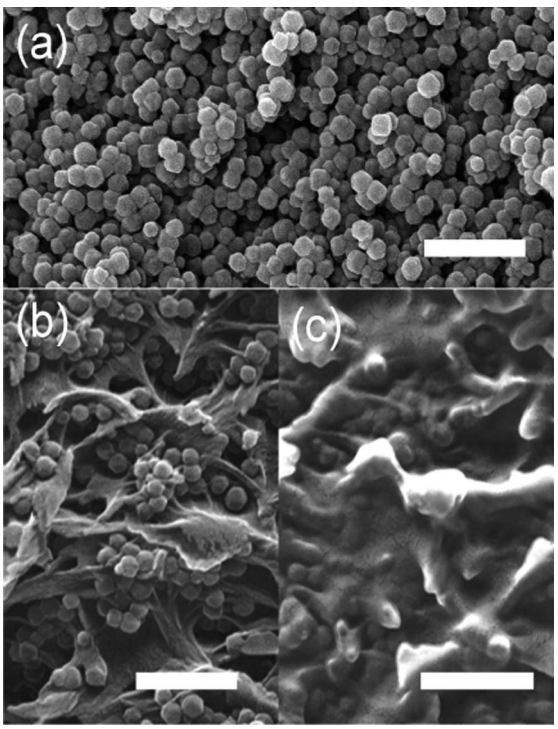

Fig. 2 SEM images of (a) pure ZIF-8 nanocrystals and (b and c) cross-section of Matrimid®–ZIF-8 composite membranes. (b) Example of poor dispersion using dried ZIF-8 nanoparticles (20 wt% loading), (c) example of good dispersion (20 wt% ZIF-8) using as synthesised ZIF-8 nanoparticles. All samples were annealed at 230 °C for 18 h under vacuum. Scale bars are 500 nm.

isotherms at 77 K (Micromeritics ASAP 2020). The physisorption of H_2, CO_2 and N_2 was also performed with a representative nanocomposite membrane with 20 wt% loading of ZIF-8 nanoparticles. The membrane (~0.1 g) was cut into small pieces. All samples were degassed under high vacuum (<10^{-6} bar) for 4 h prior to the measurement. The specific surface area (S_{BET}) was calculated based on the Brunauer–Emmett–Teller (BET) model[57] and the pore size distribution was derived from the non-linear density functional theory (DFT) model.

The local free volume of Matrimid® based membranes was measured using positron annihilation lifetime spectroscopy (PALS).[58,59] The source of positrons was provided by ^{22}Na, and

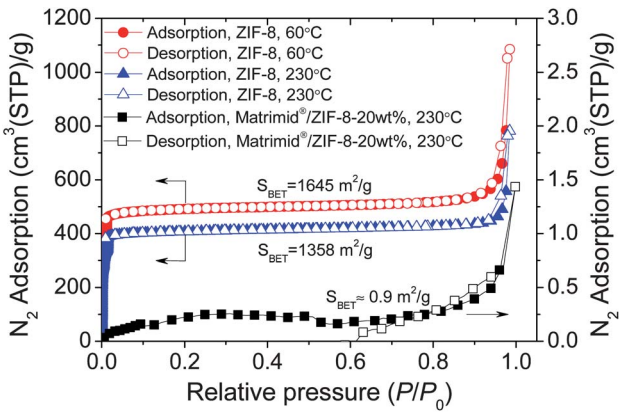

Fig. 3 N_2 adsorption and desorption isotherms of the ZIF-8 nanoparticles and Matrimid®–ZIF-8 nanocomposite membrane with 20 wt% loading. The ZIF-8 nanoparticles were annealed at 60 °C and 230 °C respectively under high vacuum for 18 h prior to N_2 adsorption measurements at 77 K.

PALS experiments were performed using a fast-fast coincidence system.[58,59] The membranes used for the PALS experiments were cut into 1 × 1 cm squares and were stacked on top of each other to produce a thickness of ~1.1 mm, enough to stop ~99% of the incident positrons. The lifetime measurements were carried out in an air-tight copper sample holder at 25 °C, with at least 5.5 million counts for all spectra. In molecular materials, a substantial fraction of the injected positrons form positronium (Ps), a metastable positron–electron bound state. The "pick-off" lifetime, τ_{po}, of the more abundant and longer lived *ortho*-positronium provides a highly accurate correspondence to the average molecular hole size, r_h, which can be calculated *via* the following semi-empirical equation:

$$\tau_{po} = 0.5\ \text{ns}\left[1 - \frac{r_h}{r_h + \delta r} + \frac{1}{2\pi}\sin\left(\frac{2\pi r_h}{r_h + \delta r}\right)\right]^{-1}. \quad (2)$$

Here, 0.5 ns is the spin-averaged lifetime of the Ps[58,59] and the positronium wave function may overlap with the wave functions of molecular electrons within a layer δr of the potential well.[60,61] The lifetime spectra were analysed using the Life Time fitting routine[62] (version 9.1) and a four finite lifetime component analysis yielded the optimum fit to the experimental data.

Table 2 Pure gas permeation properties of Matrimid®–ZIF-8 nanocomposite membranes with 20 wt% loading of ZIF-8 nanoparticles. Membrane samples were annealed at various temperatures for 18 h under vacuum

	Permeability (Barrer)				
Sample	H_2	CO_2	O_2	N_2	CH_4
Matrimid®–ZIF-8, 20 wt%, 60 °C	28.89	19.75	3.98	1.77	1.06
Matrimid®–ZIF-8, 20 wt%, 150 °C	36.38	8.78	2.81	0.42	0.23
Matrimid®–ZIF-8, 20 wt%, 180 °C	48.23	12.96	4.52	0.61	0.31
Matrimid®–ZIF-8, 20 wt%, 200 °C	56.52	12.92	4.09	0.61	0.36
Matrimid®–ZIF-8, 20 wt%, 230 °C	63.53	16.63	5.63	0.88	0.46

	Selectivity				
Sample	CO_2/N_2	CO_2/CH_4	O_2/N_2	H_2/N_2	H_2/CH_4
Matrimid®–ZIF-8, 20 wt%, 60 °C	11.1	18.6	2.2	16.3	27.3
Matrimid®–ZIF-8, 20 wt%, 150 °C	20.8	37.5	6.7	86.3	155.6
Matrimid®–ZIF-8, 20 wt%, 180 °C	21.3	41.5	7.4	79.2	154.6
Matrimid®–ZIF-8, 20 wt%, 200 °C	21.3	35.5	6.7	93.3	155.3
Matrimid®–ZIF-8, 20 wt%, 230 °C	19.0	35.8	6.4	72.5	137.0

Table 3 Pure gas permeation properties of the pure Matrimid® membrane and Matrimid®–ZIF-8 composite membranes. All membrane samples were annealed under vacuum at 230 °C for 18 h

	Permeability (Barrer)				
Sample	H_2	CO_2	O_2	N_2	CH_4
Matrimid®	32.68	8.07	2.62	0.36	0.23
Matrimid®–ZIF-8, 5 wt%	38.05	10.05	3.15	0.47	0.26
Matrimid®–ZIF-8, 10 wt%	52.56	13.67	4.64	0.63	0.45
Matrimid®–ZIF-8, 20 wt%	63.53	16.63	5.63	0.88	0.46
Matrimid®–ZIF-8, 30 wt%	112.06	28.72	10.18	1.68	1.16

	Selectivity				
Sample	CO_2/N_2	CO_2/CH_4	O_2/N_2	H_2/N_2	H_2/CH_4
Matrimid®	22.4	35.2	7.3	90.9	142.7
Matrimid®–ZIF-8, 5 wt%	21.2	39.1	6.6	80.4	148.2
Matrimid®–ZIF-8, 10 wt%	21.6	30.6	7.3	82.9	117.7
Matrimid®–ZIF-8, 20 wt%	19.0	35.8	6.4	72.5	137.0
Matrimid®–ZIF-8, 30 wt%	17.1	24.9	6.1	66.8	97.0

2.5. Gas permeation test

In this study, we focused on the mechanism of gas permeation of the nanocomposite membrane and studied the pure gas permeation using the established constant-volume variable-pressure method (the "time-lag" method).[63,64] The permeation setup is shown in Fig. S1†. An example of the pressure–time profile is also shown in Fig. S2†. The pure gas permeation experiments were performed at the feed pressure of 4 bar and room temperature (22 °C). Pure gases were tested following the sequence of H_2, O_2, N_2, CH_4, and CO_2. The gas permeability is calculated based on the following equation:[63,64]

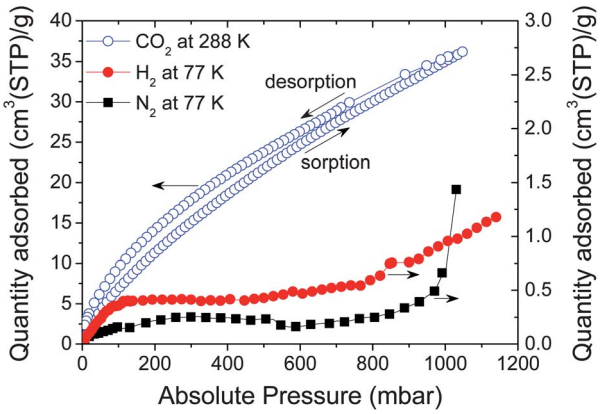

Fig. 4 Gas sorption tests of the Matrimid®–ZIF-8 nanocomposite membrane with 20 wt% loading of ZIF-8 nanoparticles. The membrane was annealed at 230 °C for 18 h and tested in pure gas permeation. Prior to gas adsorption measurement, the membrane was degassed at 110 °C for 4 h. The gas adsorption capacities were found to be at 0.05, 0.06 and 1.61 mmol g^{-1} for N_2 (77 K), H_2 (77 K) and CO_2 (288 K), respectively.

$$P = \frac{Vl}{A}\frac{T_0}{p_f p_0 T}\left(\frac{dp}{dt}\right) \quad (3)$$

where P is the permeability of the gas through the membrane, generally expressed in Barrer (1 Barrer = 10^{-10} cm^3 (STP) cm cm^{-2} s^{-1} $cmHg^{-1}$), V is the permeate volume (cm^3), l is the thickness of the membrane (cm), A is the effective area of the membrane (cm^2), p_f is the feed pressure (cmHg), p_0 is the pressure at standard state (76 cmHg), T is the absolute operating temperature (K), T_0 is the temperature at standard state (273.15 K), dp/dt is the rate of pressure increase in the permeate volume at the steady state (cmHg s^{-1}). In the experiment, the pressure rise due to the leakage was found to be negligible and hence not considered in the calculation. The error of the calculated permeability mainly originated from the variation of membrane thickness; for this study, the uncertainties of gas permeability are within ±5% and selectivity within ±7%.

The ideal selectivity ($\alpha_{A/B}$) of gas pairs, A and B, is defined as the ratio of their permeability:

$$\alpha_{A/B} = \frac{P_A}{P_B} = \left[\frac{D_A}{D_B}\right]\left[\frac{S_A}{S_B}\right] \quad (4)$$

where D_A/D_B is the diffusivity selectivity, equal to the ratio of the diffusion coefficients of gases A and B, respectively. Similarly the solubility selectivity, S_A/S_B, is the ratio of the solubility coefficients of the gases.

The time lag (θ), determined from the intercept of the steady-state region of permeate pressure with the time axis (see Fig. S2†), represents the time required for the gas to be absorbed in the polymer and diffuse through the membrane. Therefore, the diffusion coefficient (D) for a specific gas can be derived as:

Table 4 PALS parameters measured for Matrimid® membranes with different loadings of ZIF-8 at 25 °C. All membranes were annealed under vacuum at 230 °C for 18 h prior to the PALS measurements. For a brief discussion of the intensities reported here please refer to the ESI†

Sample	$\tau_{o\text{-Ps},1}$ (ns)	$r_{h,1}$ (Å)	$I_{o\text{-Ps},1}$ (%)	$\tau_{o\text{-Ps},2}$ (ns)	$r_{h,2}$ (Å)	$I_{o\text{-Ps},2}$ (%)
Matrimid®	1.19 ± 0.06	1.95 ± 0.08	1.8 ± 0.3	4.62 ± 0.08	4.57 ± 0.04	2.3 ± 0.1
Matrimid®–ZIF-8, 5 wt%	1.53 ± 0.10	2.37 ± 0.12	2.0 ± 0.1	4.99 ± 0.20	4.74 ± 0.08	2.4 ± 0.1
Matrimid®–ZIF-8, 10 wt%	1.43 ± 0.07	2.26 ± 0.08	2.3 ± 0.1	4.77 ± 0.18	4.64 ± 0.09	2.7 ± 0.1
Matrimid®–ZIF-8, 20 wt%	1.54 ± 0.05	2.39 ± 0.05	3.1 ± 0.1	4.75 ± 0.23	4.63 ± 0.11	3.0 ± 0.2
Matrimid®–ZIF-8, 30 wt%	1.67 ± 0.09	2.53 ± 0.08	3.2 ± 0.1	5.24 ± 0.12	4.86 ± 0.05	4.4 ± 0.2

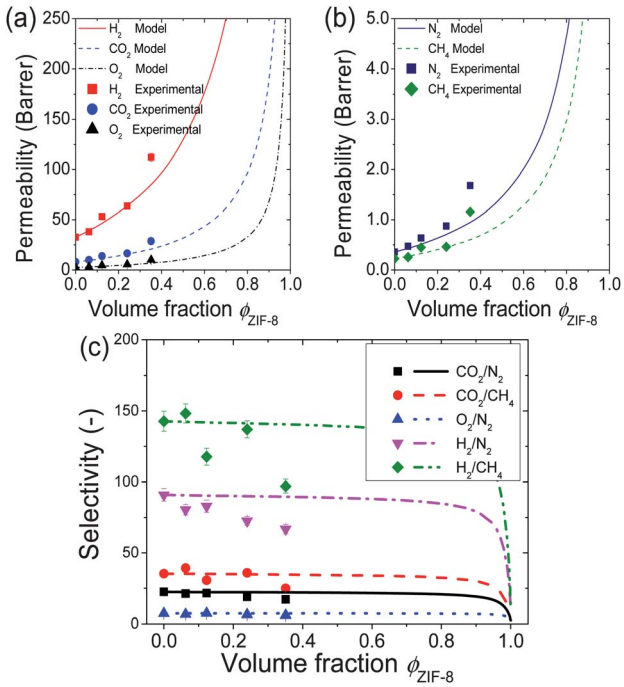

Fig. 5 Representative (a and b) gas permeability and (c) selectivity as a function of volume fraction of ZIF-8 in the Matrimid®–ZIF-8 nanocomposite membranes. Symbols: experimental data; lines: model prediction using eqn (7) and (4).

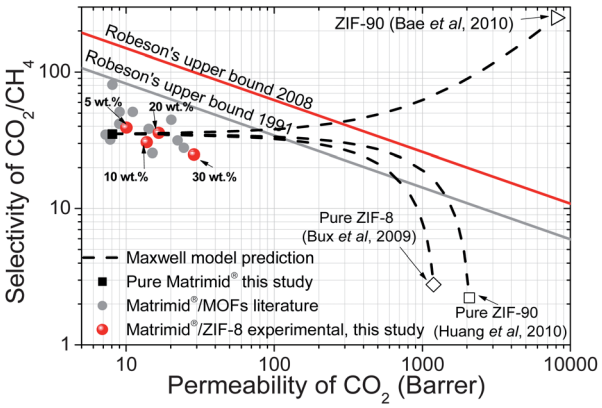

Fig. 6 CO_2/CH_4 selectivity *versus* the permeability of CO_2 of Matrimid®–ZIF mixed matrix membranes in terms of the volume fraction of ZIFs. The upper bound trade-off lines refer to Robeson's upper bound summarised in 1991 and 2008.[3,4] All three dashed lines indicate the Maxwell model prediction (eqn (7)) using the gas permeation data of the pure Matrimid® presented in this study and pure ZIF-based membrane (as marked), with pure ZIF-8 reported by Bux *et al.*,[33] pure ZIF-90 membrane reported by Huang *et al.*,[32] and submicrometer sized ZIF-90 estimated from the mixed matrix membrane by Bae *et al.*[51]

$$D = \frac{l^2}{6\theta} \tag{5}$$

Then the solubility (S) can be derived from:

$$S = \frac{P}{D} \tag{6}$$

3. Results and discussion

3.1. Characterisation of the nanocomposite membranes

The as-synthesised ZIF-8 nanoparticles were routinely characterised by various physical and chemical techniques, the results of which are provided in the ESI, Fig. S3–6†. Pure ZIF-8 nanocrystals show an average particle size of ~70 nm (Fig. S3†), with high crystallinity (Fig. S4 and S5†) and high microporosity (S_{BET} > 1300 m^2 g^{-1}, Fig. S6†).

The Matrimid®–ZIF-8 composite membranes were also characterised by various physical and chemical techniques. The membranes were transparent and flexible (Fig. S7†). We observed that the membranes with high loading of ZIF-8 became dark yellowish after annealing at temperatures above 200 °C while a similar phenomenon was observed for the pure ZIF-8 nanoparticles, possibly due to the decomposition of ZIF-8.[65] Yet the membranes were still transparent and flexible. The apparent density of the composite membranes (Table 1) as estimated from the mass with thickness and area varied between 1.1 and 1.2 g cm^{-3}, which is approximate to the theoretical density as calculated based on the loading of ZIF-8 nanoparticles. The SEM micrographs of the cross-sectional morphology of membranes at low magnification can be found in Fig. S8†.

The high-magnification SEM micrographs of pure ZIF-8 nanocrystals and the cross-section of representative membranes are shown in Fig. 2. We carried out control experiments using dried nanoparticles which were not readily re-dispersible in the solvent even with ultrasonication. As shown in Fig. 2b, for the membrane using dried ZIF-8 nanoparticles (20 wt% loading), we can see the aggregation of ZIF-8 forming a grape-like morphology and consequently poor adhesion at the MOF–polymer interface. In some other trial and error experiments, we also observed the poor dispersion if the nanoparticles had been aged in methanol or chloroform for several days instead of using newly prepared ones. Such aggregation is consistent with the initial report by Cravillon *et al.*[55] and is further confirmed by recent studies by Yang[50] and Liu *et al.*[54] Using as-synthesised

Table 5 Comparison of measured and predicted gas permeation properties of Matrimid®–ZIF-8 composite membranes. All samples were annealed at 230 °C for 18 h under vacuum

Loading of ZIF-8 (wt%)	ϕ_{ZIF-8}	CO_2 permeability (Barrer)		CO_2/CH_4 selectivity	
		Experimental	Model	Experimental	Model
0	0	8.07 ± 0.28	8.07	35.2 ± 1.73	35.2
5	0.06	10.05 ± 0.32	9.6	39.1 ± 1.77	35.1
10	0.12	13.78 ± 0.49	11.4	30.6 ± 1.55	35.0
20	0.24	16.63 ± 0.52	15.5	35.8 ± 1.57	34.8
30	0.35	28.72 ± 1.02	20.8	24.9 ± 1.25	34.6
40	0.46	—	27.7	—	34.4
50	0.56	—	37.3	—	34.1
90	0.92	—	227.3	—	28.9
Pure ZIF-8[a]	1.0	1192	1192	2.8	2.8

[a] Data calculated from the gas permeance of pure ZIF-8 membrane by Bux *et al.*[33] For a detailed summary of data see Table S1†.

ZIF-8 nanoparticles, we can obtain good dispersion and adhesion of ZIF-8 nanocrystals within the polymer matrix (Fig. 2c) (up to ZIF-8 loading level of 30 wt%). Large clusters or aggregates of ZIF-8 particles were not observable in SEM. The "sieve in a cage" morphology[16,18] was not seen under these optimised conditions. At higher loading of 40 wt%, the polymer appears to be still continuous as observed in SEM although the membrane became brittle and cracked easily. The method of direct mixing of as-synthesised nanoparticles in this study considerably improved the observed mixing and dispersion in polymer matrix, compared to previous work on such mixed matrix systems.[53]

Wide-angle X-ray diffraction patterns of the pure polymer and composite membranes are presented in Fig. S9†. The pure Matrimid® polymer membrane is completely amorphous. For all the Matrimid®–ZIF-8 composite membranes with different loadings, the crystalline structures of ZIF-8 nanoparticles are clearly the same as that of pure ZIF-8. The crystallite thickness or diameter of the ZIF-8 nanocrystals in the composite membrane was quantitatively obtained by the Scherrer equation,[56] giving average crystallite sizes in the range of 50–60 nm as summarised in Table 1. This size is approximate to the size of pure ZIF-8 nanocrystals observed under the SEM (Fig. 2) and slightly smaller than that determined by XRD pattern (69 nm, Fig. S4†).

FTIR analyses were also carried out and the absorption peaks could be assigned to ZIF-8 and Matrimid® respectively (Fig. S10†), indicating that there were no strong chemical interactions between the ZIF-8 nanoparticles and the polymer.

The nitrogen adsorption–desorption isotherms of the ZIF-8 nanoparticles and a representative Matrimid®–ZIF-8 composite membrane with 20 wt% loading are shown in Fig. 3. The BET surface area and micropore volume of the ZIF-8 are as high as 1645 $m^2\ g^{-1}$ and 0.70 $cm^3\ g^{-1}$, respectively. Annealing at 230 °C resulted in a slight decrease of the surface area to 1358 $m^2\ g^{-1}$ and smaller micropore volume at 0.58 $cm^3\ g^{-1}$. Such a decline was possibly due to the decomposition of some ZIF-8 nanoparticles when activated at a higher temperature,[65] but importantly we confirmed that the microporous structure was maintained. The pore size distribution as estimated from a non-linear density functional theory (DFT) model gave a pore diameter of 10.8 Å (Fig. S6†), which is consistent with the pore diameter (11.6 Å) of the sodalite cage in pristine ZIF-8.[41] Notably, as for the composite membrane with 20 wt% loading of ZIF-8, the BET surface area as measured was found to be only about 0.9 $m^2\ g^{-1}$, which is at least three orders of magnitude lower than that of pure ZIF-8 nanoparticles. This low surface area is mainly due to the adsorption of N_2 on the bulk surface of the membrane. This finding provides direct evidence that the ZIF-8 nanoparticles were indeed in excellent adhesion with the polymer matrix and with minimal defects at the interfaces (which would give high adsorption).

The glass transition temperature of the pure polymer and nanocomposite membranes were analysed by DMA as presented in Table 1 and Fig. S11†. The glass transition temperature of the pure Matrimid® polymer is 330 °C, in the range reported in the literature (generally 300–340 °C depending on the method of measurement).[18,66] With the increased loading of ZIF-8 in the composite, the T_g increases from 330 °C to 346 °C at 10 wt% loading of ZIF-8, to around 349 °C at 30 wt% loading. A similar observation of increase of T_g was reported for the mixed matrix membrane of Matrimid® with carbon molecular sieves (CMS).[18]

For both the polymer and ZIFs nanocrystals, the residual solvent could have a significant effect on the porosity of the membrane, and consequently the gas permeation properties could be affected. Particularly, since we used the as-synthesised ZIF-8 colloidal nanoparticles for the membrane preparation in this study, residual solvent or reactant molecules could be trapped in the nanocrystals during synthesis and post-treatment, hence blocking the pores and channels of the ZIFs. To completely remove these solvents and guest molecules, conventional annealing under vacuum or on stream activation with increasing temperature would work.[36] Furthermore, annealing could also change the properties of the composite membranes, for example, the opening of pores that are accessible to gases and the removal of voids between the polymer and ZIF nanocrystals. The glass transition temperatures of a series of composite membranes with ZIF-8 loading of 20 wt% at various annealing temperatures were measured by DMA (Fig. S12†). At lower annealing temperatures of 150–230 °C, T_g was around 343 °C. On annealing at higher temperatures (>260 °C), T_g showed a slight decrease to 336 °C, possibly due to the poor adhesion between the polymer and ZIF-8 at higher annealing temperatures, which could originate from slight decomposition of ZIF-8.[65] Heat treatment above T_g was not attempted in this study as the nanocomposite membranes became very brittle when the annealing temperature exceeded 300 °C.

3.2. Effect of annealing temperature on gas transport properties

Here, we compare the gas permeation properties of the pure polymer and composite membranes with various loadings that were annealed at different temperatures. For the Matrimid® polymer membrane, the gas permeation data are presented in Table S3 and Fig. S13†. At low annealing temperatures, the selectivity was relatively low; after exposure to high temperature treatment, both the permeability and selectivity were stabilised. We can see the molecular sieving effect with gas permeability following the order of the kinetic diameter of the respective gas molecules: H_2 (2.89 Å) > CO_2 (3.3 Å) ≫ O_2 (3.46 Å) > N_2 (3.6 Å) > CH_4 (3.8 Å). In contrast, the gas permeation of the composite membranes containing 20 wt% loading of ZIF-8 nanoparticles shows different behaviour as presented in Table 2.

Similar to the pure polymer membrane, the composite membranes dried at low temperature were not selective, possibly due to the presence of residual solvents trapped among the polymer chains and interfacial defects between ZIF-8 nanoparticles and the polymer. With the increase in annealing temperature, the residual solvent molecules are expected to be completely removed from the polymer, and consequently the polymer became more selective with an increase in permeability. For the composite membrane with ZIF-8 loading of 30 wt%, similar results were obtained. However, annealing at high temperatures could result in lower performance. At an annealing temperature of 300 °C, the permeability of H_2 and CO_2 increased to 144.5 and 29.2 Barrer, respectively, while the permeability of N_2 and CH_4 also increased to 4.4 and 4.6 Barrer, respectively. Therefore, the ideal selectivity of all gas pairs decreased, *i.e.* the selectivity of H_2/CH_4 and CO_2/CH_4 significantly decreased to 31.4 and 6.3, respectively. Detailed data are given in Table S4.†

3.3. Effect of ZIF-8 loading on gas transport properties

3.3.1. Gas permeability and selectivity. Table 3 presents the gas transport data of annealed membranes prepared from the pure polymer and composite membranes with various loadings. For all membranes, the permeabilities of various gases follow the order dictated by the kinetic diameter. As the ZIF-8 loading increases up to 20 wt%, the permeability of H_2 and CO_2 increased to two times that of the pure polymer while we also see moderate increase of permeability of O_2, N_2 and CH_4. Consequently the selectivity was relatively similar to the neat polymer. The selectivities of H_2/N_2 and H_2/CH_4 showed slight decreases as a function of the ZIF-8 loading. At high loadings, *i.e.* 30 wt%, the permeability increased to three times that of the pure polymer, however, the selectivity of typical gas pairs decreased.

3.3.2. Solubility and diffusion coefficient. The gas permeation data were further analysed and the diffusion coefficient and solubility of gases in the membrane (for an upstream pressure of 4 bar) could be derived; representative data are shown in Fig. S14†. The uncertainty of diffusion coefficient was within ±12%, although in the case of H_2 it is slightly higher (maximum ±20%) because of the experimental error associated with time lag. Again, the diffusion coefficients of various gases are approximately correlated to the kinetic diameter, while the solubility of gases in the polymer is strongly dependent on the critical temperature of the gas molecules, following the order of CO_2 (304.19 K) ≫ CH_4 (190.9 K) > O_2 (154.6 K) > N_2 (126.3 K) > H_2 (33.20 K). These data are in agreement with the literature on Matrimid® polymer.[18,66] As the loading of ZIF-8 increases, both the diffusion coefficient and the solubility of H_2 increased to several times that of the pure polymer, which could be attributed to the high capacity of adsorption and diffusion of H_2 in ZIF-8.[41] The major contribution to the increase in CO_2 permeability comes from the diffusion coefficient while the solubility of CO_2 is relatively constant. The crystallographic pore aperture of ZIF-8 crystals is ~3.4 Å, ideally, it would allow the transport of gas molecules with smaller kinetic diameter, such as H_2 (2.89 Å) and CO_2 (3.3 Å), blocking the large molecules including N_2 (3.64 Å) or CH_4 (3.8 Å). However, an increase of both solubility and diffusion coefficients of N_2 and CH_4 was observed accompanied with a moderate increase of permeability. These data suggest the interaction between these gas molecules and ZIF-8 crystals,[42] and the flexible pore structure of ZIF-8 cages (*via* gate-opening, see Fig. S6†) permits the diffusion of molecules with larger kinetic diameters, as suggested in the literature.[33,67,68] The increased free volume of the polymer also contributes to the overall diffusion of N_2 and CH_4 as indicated by PALS analysis.

Direct gas sorption was measured *via* a Micromeritics ASAP 2020 up to pressures of 1 bar. Fig. 4 shows the gas sorption measurements of H_2 (77 K), N_2 (77 K) and CO_2 (288 K) of a representative polymer–ZIF-8 composite membrane with 20 wt% loading. The gas sorption data are sufficient to confirm that the adsorption of H_2 and N_2 was found to be quite low compared to the pure ZIF-8 sample, further verifying the defect-free interface between the ZIF-8 and polymer. In contrast, the amount of CO_2 uptake at 288 K is appreciably higher than that of N_2 and H_2; this is accounted for by the high solubility of CO_2 in the composite membrane.

A sorption or solubility value for CO_2 of 0.52 cm^3 (STP)/(cm^3 cmHg) at 1 bar is determined directly from the slope in Fig. 4. In contrast, the solubility derived from gas permeation at the higher operating pressure of 4 bar gave values of 0.15 cm^3 (STP)/(cm^3 cmHg) (Fig. S14†). However the absolute values of the indirectly measured solubilities could have been biased by concentration dependent diffusion across the membrane. Nonetheless this confirms that the sorption approaches an asymptotic value at higher pressures with only slow mode contributions to the adsorption isotherm, though as indicated in the literature,[66,69] this asymptote is often reached at higher pressures than used in this study. The direct sorption measurement made at 1 bar reflects the dual mode sorption regime, with Langmuir adsorption contributions, from the gas sorption in free volume of polymer and saturation of nanocages of ZIF-8.[70]

3.3.3. Measurement of the local free volume by PALS. In Table 4 we report the two *o*-Ps lifetimes (and their respective intensities) and the average radii of the free volume elements measured for Matrimid® membranes with different ZIF-8 loading levels. The presence of two distinct *o*-Ps lifetimes in the pure Matrimid® membrane suggests that the distribution of free volume is bimodal.[71] Structurally, the ZIF-8 inclusions possess large pores, 11.6 Å in diameter, which are connected through by small apertures, 3.4 Å in diameter.[41] The lifetimes of *o*-Ps

annihilating within such pores would be of the order of 5 ns and 1 ns for the larger and smaller pores, respectively. These lifetimes are too similar to the two *o*-Ps lifetimes measured in the pure Matrimid® membrane, meaning that they cannot be reliably resolved as separate lifetime components in the spectra of the composite membranes. Therefore, the PALS measurements reflect the changes in molecular packing of the base Matrimid® polymer.

From Table 4 we can see that there is a systematic increase in the shorter *o*-Ps lifetime as a function of the increasing ZIF-8 loading (with the exception of the membranes containing 5 wt% of ZIF-8), while the changes in the longer *o*-Ps are significantly less pronounced. Our PALS measurements, therefore, illustrate that the ZIF-8 inclusions alter the molecular packing of the polyimide based membranes, leading to an increase in the average sizes of the free volume elements. The effect of the ZIF-8 inclusions on the permeation properties of the membranes is, therefore, two-fold: they reduce the efficiency of the molecular packing of the base Matrimid® polymer, while gas molecules can freely diffuse though the pores of the ZIF-8 cages, both of which lead to an increase in the permeability of the composite membranes.

3.3.4. Modelling. For the polymer/molecular sieves nanocomposite membranes, the Maxwell model is usually used to predict the gas permeability.[16] This well-known model was initially presented by Maxwell in 1873 to predict the conduction of a dielectric through heterogeneous media.[72] The gas permeation through a mixed matrix membrane under the pressure driving force is analogous to the conduction of a dielectric in heterogeneous media under an electric potential:

$$P_{\text{eff}} = P_{\text{C}}\left[\frac{P_{\text{D}} + 2P_{\text{C}} - 2\phi_{\text{D}}(P_{\text{C}} - P_{\text{D}})}{P_{\text{D}} + 2P_{\text{C}} + \phi_{\text{D}}(P_{\text{C}} - P_{\text{D}})}\right] \quad (7)$$

where P_{eff} is the effective permeability of the composite membrane, P_{C} and P_{D} represent the permeability of the continuous phase (polymer) and dispersed phase (ZIF-8 here), respectively. With the permeability, the ideal selectivity of gas pairs ($P_{\text{A}}/P_{\text{B}}$) could also be predicted. Ideally, the model is applicable to diluted suspensions of spherical particles in a matrix without consideration of non-ideal cases, such as the particle size distribution, shape, interfacial voids, aggregation of particles, pore blockage, and rigidification of surrounding polymer chains.

The gas permeation data for the pure ZIF-8 membrane is re-calculated from the pure gas permeation data reported by Bux *et al.*[33] The gas flux of H_2, CO_2, O_2, N_2, and CH_4 through the 30 μm thickness membrane are 6.04, 1.33, 1.04, 0.52, 0.48 × 10^{-8} mol m^{-2} s^{-1} Pa^{-1}, corresponding to intrinsic gas permeability of 5411, 1192, 932, 466, 430 Barrer, respectively (Table S1†).[35,42] The model predictions match well with the experimental data, although there appears to be a systematic underprediction of the permeability for all the gases (Fig. 5). This correlates well with the PALS observation of an enhanced polymer free volume (and hence larger contribution to permeability) with ZIF-8 loading, since this consideration and detailed dispersion characteristics are not included in the idealized Maxwell model.

The CO_2/CH_4 separation performance is also compared with the Robeson's upper bound as shown in Fig. 6 with representative data shown in Table 5. The Maxwell model predictions in this figure suggest that gas permeability of the composite membrane is considerably enhanced while the selectivity of the composite membrane remains constant at reasonable range of loadings if the fillers are far more porous than the polymer matrix. The gas permeation behaviour at high loading of ZIF-8 can be predicted by the Maxwell model. Interestingly, the CO_2/CH_4 selectivity is maintained above 30 when the loading increases up to 90 wt% (this is an ideal estimation). We also predict in Fig. 6 the gas permeation of Matrimid® composites with some other types of ZIFs, *i.e.* ZIF-90; the enhancement of gas permeability at lower loading of ZIFs is similar for both highly or low selective ZIFs as fillers.

The permeability and selectivity could be determined by the coupling of the polymer and ZIFs. Bae *et al.*[51] observed enhanced permeability and selectivity when ZIF-90 crystals at sub-nanometer size were incorporated into a 6FDA-DAM polymer. They estimated that the CO_2 permeability and CO_2/CH_4 selectivity of ZIF-90 is 8000 Barrer and 250, respectively. This permeation data is quite different from the data of pure ZIF-90 membrane (1192 Barrer, selectivity of 2.8) as reported by Huang *et al.*[32] Recently, Yang *et al.*[50] reported that addition of ZIF-7 nanoparticles into a polybenzimidazole (PBI) matrix enhanced the permeability of H_2 and selectivity over CO_2, which was also higher than that predicted by the Maxwell model. They attributed the increase of selectivity to the interaction of ZIF-7 with PBI.

Nevertheless, the current model prediction indicates that it is possible to achieve high gas separation performance by adopting the right combination of a highly selective MOF with a highly permeable polymer, as suggested by Keskin and Sholl.[46] Potent high permeability polymer candidates could include the 6FDA-DAM polymer (*e.g.* as in the study by Bae *et al.*[51]). Alternatively recent significant progress has been achieved on developing highly permeable polymers, such as polymers of intrinsic microporosity (PIMs).[6–9] Using a similar method of dispersing the ZIF nanoparticles established in this study, further work on the combination of the highly permeable PIMs and ZIFs to achieve high performance of gas separation is underway and will be reported in the near future.

4. Conclusion

In summary, we report the preparation of nanocomposite membranes composed of a polymer matrix which features good dispersion and adhesion of ZIF-8 nanoparticles within the polymer. We show that annealing the polymer nanocomposite membranes under vacuum has a positive impact on their gas permeation properties, as a consequence of residual solvent removal from the matrices coupled with the activation of ZIF-8 nanocrystals. Upon increasing the loading of ZIF-8 nanoparticles in the mixed matrix membranes, the gas permeability increases substantially while the selectivity remains largely unchanged in comparison with the pure polymer membrane. Gas adsorption studies further confirmed that the selective gas transport is predominated by the polymeric phase. Additionally, the PALS analyses indicated that incorporation of ZIF-8 reduces the efficiency of the molecular packing of the polymer, while gas molecules can freely diffuse though the pores of the ZIF-8 cages,

both of which lead to an increase in the permeability of the composite membranes. The experimental data are essentially predicted by the Maxwell model, but with deviations that can be associated with corrections for a small non-ideal distribution of nanoparticles and the influence of ZIF-8 loading on the polymeric free volume. An important finding is that the projected capability of the dispersion method used in this study has the potential to enhance the permeability to the limit of the Robeson upper bound by matching highly permeable polymer and the intimate mixing of selective fillers.

Acknowledgements

We acknowledge financial support through an NPRP grant by the Qatar National Research Fund (QNRF) and the Engineering and Physical Sciences Research Council (EPSRC, UK). Q.S. acknowledges a PhD scholarship from the China Scholarship Council. The authors thank Mr Mark Salisbury at Huntsman Advanced Materials for kindly supplying the Matrimid® 5218 polymer and Dr John Gearing for access to the DMA analyser.

References

1 R. W. Baker, *Ind. Eng. Chem. Res.*, 2002, **41**, 1393–1411.
2 B. D. Freeman, *Macromolecules*, 1999, **32**, 375–380.
3 L. M. Robeson, *J. Membr. Sci.*, 1991, **62**, 165–185.
4 L. M. Robeson, *J. Membr. Sci.*, 2008, **320**, 390–400.
5 W. J. Koros and R. Mahajan, *J. Membr. Sci.*, 2000, **175**, 181–196.
6 N. Du, H. B. Park, M. M. Dal-Cin and M. D. Guiver, *Energy Environ. Sci.*, 2012, **5**, 7306–7322.
7 P. M. Budd, E. S. Elabas, B. S. Ghanem, S. Makhseed, N. B. McKeown, K. J. Msayib, C. E. Tattershall and D. Wang, *Adv. Mater.*, 2004, **16**, 456–459.
8 P. M. Budd, K. J. Msayib, C. E. Tattershall, B. S. Ghanem, K. J. Reynolds, N. B. McKeown and D. Fritsch, *J. Membr. Sci.*, 2005, **251**, 263–269.
9 N. Du, H. B. Park, G. P. Robertson, M. M. Dal-Cin, T. Visser, L. Scoles and M. D. Guiver, *Nat. Mater.*, 2011, **10**, 372–375.
10 S. J. Metz, M. H. V. Mulder and M. Wessling, *Macromolecules*, 2004, **37**, 4590–4597.
11 A. Car, C. Stropnik, W. Yave and K. V. Peinemann, *Adv. Funct. Mater.*, 2008, **18**, 2815–2823.
12 H. Lin, E. Van Wagner, R. Raharjo, B. D. Freeman and I. Roman, *Adv. Mater.*, 2006, **18**, 39–44.
13 H. Lin, E. Van Wagner, B. D. Freeman, L. G. Toy and R. P. Gupta, *Science*, 2006, **311**, 639–642.
14 H. B. Park, C. H. Jung, Y. M. Lee, A. J. Hill, S. J. Pas, S. T. Mudie, E. Van Wagner, B. D. Freeman and D. J. Cookson, *Science*, 2007, **318**, 254–258.
15 J. D. Wind, D. R. Paul and W. J. Koros, *J. Membr. Sci.*, 2004, **228**, 227–236.
16 T. S. Chung, L. Y. Jiang, Y. Li and S. Kulprathipanja, *Prog. Polym. Sci.*, 2007, **32**, 483–507.
17 T. C. Merkel, B. D. Freeman, R. J. Spontak, Z. He, I. Pinnau, P. Meakin and A. J. Hill, *Science*, 2002, **296**, 519–522.
18 D. Q. Vu, W. J. Koros and S. J. Miller, *J. Membr. Sci.*, 2003, **211**, 311–334.
19 D. L. Gin and R. D. Noble, *Science*, 2011, **332**, 674–676.
20 P. Zavala-Rivera, K. Channon, V. Nguyen, E. Sivaniah, D. Kabra, R. H. Friend, S. K. Nataraj, S. A. Al-Muhtaseb, A. Hexemer, M. E. Calvo and H. Miguez, *Nat. Mater.*, 2012, **11**, 53–57.
21 S. R. Reijerkerk, M. H. Knoef, K. Nijmeijer and M. Wessling, *J. Membr. Sci.*, 2010, **352**, 126–135.
22 J.-R. Li, R. J. Kuppler and H.-C. Zhou, *Chem. Soc. Rev.*, 2009, **38**, 1477–1504.
23 A. R. Millward and O. M. Yaghi, *J. Am. Chem. Soc.*, 2005, **127**, 17998–17999.
24 J. C. Tan and A. K. Cheetham, *Chem. Soc. Rev.*, 2011, **40**, 1059–1080.
25 K. Sumida, D. L. Rogow, J. A. Mason, T. M. McDonald, E. D. Bloch, Z. R. Herm, T.-H. Bae and J. R. Long, *Chem. Rev.*, 2011, **112**, 724–781.
26 M. P. Suh, H. J. Park, T. K. Prasad and D.-W. Lim, *Chem. Rev.*, 2011, **112**, 782–835.
27 J.-R. Li, J. Sculley and H.-C. Zhou, *Chem. Rev.*, 2011, **112**, 869–932.
28 R. B. Getman, Y.-S. Bae, C. E. Wilmer and R. Q. Snurr, *Chem. Rev.*, 2011, **112**, 703–723.
29 A. Bétard and R. A. Fischer, *Chem. Rev.*, 2011, **112**, 1055–1083.
30 H. Hayashi, A. P. Côté, H. Furukawa, M. O'Keeffe and O. M. Yaghi, *Nat. Mater.*, 2007, **6**, 501–506.
31 S. R. Venna and M. A. Carreon, *J. Am. Chem. Soc.*, 2010, **132**, 76–78.
32 A. Huang, W. Dou and J. Caro, *J. Am. Chem. Soc.*, 2010, **132**, 15562–15564.
33 H. Bux, F. Liang, Y. Li, J. Cravillon, M. Wiebcke and J. Caro, *J. Am. Chem. Soc.*, 2009, **131**, 16000–16001.
34 Y. Li, F. Liang, H. Bux, W. Yang and J. Caro, *J. Membr. Sci.*, 2010, **354**, 48–54.
35 H. Bux, A. Feldhoff, J. Cravillon, M. Wiebcke, Y. S. Li and J. Caro, *Chem. Mater.*, 2011, **23**, 2262–2269.
36 Y. S. Li, F. Y. Liang, H. Bux, A. Feldhoff, W. S. Yang and J. Caro, *Angew. Chem., Int. Ed.*, 2010, **49**, 548–551.
37 A. Huang and J. Caro, *Angew. Chem., Int. Ed.*, 2011, **50**, 4979–4982.
38 A. Huang, H. Bux, F. Steinbach and J. Caro, *Angew. Chem., Int. Ed.*, 2010, **49**, 4958–4961.
39 H. Bux, C. Chmelik, R. Krishna and J. Caro, *J. Membr. Sci.*, 2011, **369**, 284–289.
40 A. W. Thornton, D. Dubbeldam, M. S. Liu, B. P. Ladewig, A. J. Hill and M. R. Hill, *Energy Environ. Sci.*, 2012, **5**, 7637–7646.
41 K. S. Park, Z. Ni, A. P. Côté, J. Y. Choi, R. Huang, F. J. Uribe-Romo, H. K. Chae, M. O'Keeffe and O. M. Yaghi, *Proc. Natl. Acad. Sci. U. S. A.*, 2006, **103**, 10186–10191.
42 M. C. McCarthy, V. Varela-Guerrero, G. V. Barnett and H. K. Jeong, *Langmuir*, 2010, **26**, 14636–14641.
43 Z. Lai, G. Bonilla, I. Diaz, J. G. Nery, K. Sujaoti, M. A. Amat, E. Kokkoli, O. Terasaki, R. W. Thompson, M. Tsapatsis and D. G. Vlachos, *Science*, 2003, **300**, 456–460.
44 J. Caro, M. Noack, P. Kölsch and R. Schäfer, *Microporous Mesoporous Mater.*, 2000, **38**, 3–24.
45 J. Caro, *Curr. Opin. Chem. Eng.*, 2011, **1**, 77–83.
46 S. Keskin and D. S. Sholl, *Energy Environ. Sci.*, 2010, **3**, 343–351.
47 E. V. Perez, K. J. Balkus Jr, J. P. Ferraris and I. H. Musselman, *J. Membr. Sci.*, 2009, **328**, 165–173.
48 Y. Zhang, I. H. Musselman, J. P. Ferraris and K. J. Balkus Jr, *J. Membr. Sci.*, 2008, **313**, 170–181.
49 S. Basu, A. Cano-Odena and I. F. J. Vankelecom, *J. Membr. Sci.*, 2010, **362**, 478–487.
50 T. Yang, Y. Xiao and T. S. Chung, *Energy Environ. Sci.*, 2011, **4**, 4171–4180.
51 T.-H. Bae, J. S. Lee, W. Qiu, W. J. Koros, C. W. Jones and S. Nair, *Angew. Chem., Int. Ed.*, 2010, **49**, 9863–9866.
52 C. Zhang, Y. Dai, J. R. Johnson, O. Karvan and W. J. Koros, *J. Membr. Sci.*, 2012, **389**, 34–42.
53 M. J. C. Ordoñez, K. J. Balkus Jr, J. P. Ferraris and I. H. Musselman, *J. Membr. Sci.*, 2010, **361**, 28–37.
54 X.-L. Liu, Y.-S. Li, G.-Q. Zhu, Y.-J. Ban, L.-Y. Xu and W.-S. Yang, *Angew. Chem., Int. Ed.*, 2011, **50**, 10636–10639.
55 J. Cravillon, S. Münzer, S. J. Lohmeier, A. Feldhoff, K. Huber and M. Wiebcke, *Chem. Mater.*, 2009, **21**, 1410–1412.
56 A. L. Patterson, *Phys. Rev.*, 1939, **56**, 978–982.
57 S. Brunauer, P. H. Emmett and E. Teller, *J. Am. Chem. Soc.*, 1938, **60**, 309–319.
58 Y. C. Jean, P. E. Mallon and D. M. Schrader, *Positron and Positronium Chemistry*, World Scientific, River Edge, NJ, 2003.
59 D. M. Schrader and Y. C. Yean, *Positron and Positronium Chemistry*, Elsevier, Amsterdam, 1988.
60 S. J. Tao, *J. Chem. Phys.*, 1972, **56**, 5499–5510.
61 M. Eldrup, D. Lightbody and J. N. Sherwood, *Chem. Phys.*, 1981, **63**, 51–58.
62 J. Kansy, *Nucl. Instrum. Methods Phys. Res., Sect. A*, 1996, **374**, 235–244.
63 S. A. Stern, *J. Membr. Sci.*, 1994, **94**, 1–65.

64 H. Lin and B. Freeman, in *Springer Handbook of Materials Measurement Methods*, Springer, Berlin, Heidelberg, 2006, pp. 283–397.
65 J.-C. Tan, B. Civalleri, C.-C. Lin, L. Valenzano, R. Galvelis, P.-F. Chen, T. D. Bennett, C. Mellot-Draznieks, C. M. Zicovich-Wilson and A. K. Cheetham, *Phys. Rev. Lett.*, 2012, **108**, 095502.
66 T.-S. Chung, S. S. Chan, R. Wang, Z. Lu and C. He, *J. Membr. Sci.*, 2003, **211**, 91–99.
67 S. A. Moggach, T. D. Bennett and A. K. Cheetham, *Angew. Chem.*, 2009, **121**, 7221–7223.
68 J. C. Tan, T. D. Bennett and A. K. Cheetham, *Proc. Natl. Acad. Sci. U. S. A.*, 2010, **107**, 9938–9943.
69 T. T. Moore and W. J. Koros, *J. Appl. Polym. Sci.*, 2007, **104**, 4053–4059.
70 J. M. Simmons, H. Wu, W. Zhou and T. Yildirim, *Energy Environ. Sci.*, 2011, **4**, 2177–2185.
71 V. P. Shantarovich, I. B. Kevdina, Y. P. Yampolskii and A. Y. Alentiev, *Macromolecules*, 2000, **33**, 7453–7466.
72 J. C. Maxwell, *A Treatise on Electricity and Magnetism*, Oxford Univ. Press, London, 1873.